Bridge Model for Individualized Digital NasoAlveolar Molding using Uniform Cross-Section Elliptic Segment

Hathaichanok Parakarn[1], Buddhathida Wangsrimongkol[2], Nawapak Eua-Anant[3] and Tatpong Katanyukul[4[0000-0003-3586-475X]]

[1,2] Division of Orthodontics, Faculty of Dentistry, Khon Kaen University, Thailand
[3,4] Department of Computer Engineering, Faculty of Engineering, Khon Kaen University, Thailand
Corresponding email: tatpong@kku.ac.th

Abstract. Digital orthodontics has emerged as a new paradigm of NasoAlveolar Molding (NAM). NAM is a well adopted adjunctive therapy before undergoing a lip surgery in patients with cleft lip and palate. Its mechanism is to apply differential force through a NAM plate. Conventional NAM uses a single plate, but with multiple adjustments. This causes high burden of care on patients and their families. Employing intra-oral scan and CAD/CAM, digital NAM simplifies NAM procedure and lessens clinical chair side. This also reduces a risk associated to mouth casting and allows plate reproducibility (in case of accidentally broken plates). However, early digital NAM requires design and fabrication of multiple plates throughout the process. A recent study proposes individualized Digital NAM (iDNAM) using biomechanics insight to minimize a number of plates. iDNAM has been shown to be clinically effective. Nonetheless iDNAM in its current state requires a personnel with craniofacial expertise and proficiency in 3D computer modeling.

This article presents a pilot study toward an automatic iDNAM-plate design, using ellipse and non-parametric cross-section models. The approach takes advantages of specific data characteristics, allowing low-computation techniques to achieve three-dimension surface generation.

The resulting design was assessed to provide a viable bridge model, one of the most challenging parts in plate design. This also supports our hypothesis of the elliptic-segment pattern of an alveolar ridge and shows prospect of our approach in a coveted fully automatic iDNAM-plate design.

Keywords: NasoAlveolar Molding, iDNAM, Alveolar Ridge Approximation, Elliptic Model, Non-Parametric Model, Cross-Section Model, Three-Dimension Geometry, CAD/CAM in Dentistry, Computational Science in Health Care

1 Introduction

Cleft lip and palate (CLP) is a common congenital craniofacial defect affecting the lips and oral cavity, with an incidence rate of approximately one in every 700 births[1]. This condition is caused by a variety of factors, including environmental, genetic, or a combination of both [2]. Patients with unilateral cleft lip and palate (UCLP) exhibit an

asymmetrical alar base and columella, abnormal nasal cartilage morphology, and nasal tip deviation toward the noncleft side [3].

NasoAlveolar Molding (NAM)[3–6] has long been a well adopted adjunctive therapy for patients with CLP before undergoing a primary lip surgery. Its key mechanism uses a NAM plate to apply differential force. The force is to guide the movement of the two separated alveolar segments. So that they becomes sufficiently close to each other, providing a more favorable condition for the lip surgery.

The period for the ideal nasal cartilage molding was during the first 6 weeks of age, as advocated by Matsuo et al [7]. This study showed the role of preoperative nasal molding in changing the memory of deformed nasal cartilage. Taking advantages of the higher level of hyaluronic acid, which gradually diminishes after a few months of birth. Conventional NAM technique uses a single plate, but is adjusted and modified to reflect the ongoing anatomical movement and the patient's growth. In addition to the weekly appointments for the family, this technique requires specific laboratory work for appliance fabrication, and significant clinical chair time for appliance adjustment and activation. This poses a higher burden of care on patients and their families.

Using an intra-oral scanner and CAD/CAM technology is an emerging field in cleft care and has recently been adopted into NAM therapy [8, 9]. This technique can simplify the NAM procedure, save time, and allow for reproducibility (beneficial in case of accidentally broken plates), helping offset the limitations of the conventional method. However, early digital NAM techniques [10–17] require the design and fabrication of multiple plates throughout the course and rely on an expensive specialized CAD software.

Recent studies [18–21] propose individualized Digital NAM (iDNAM), a new digital NAM system. The iDNAM workflow utilizes a free software with affordable dental modules that allows virtual alveolar segmentation, NAM plate design, and fabrication. Insight into biomechanics and interplay between a NAM plate and the subjected palates reveals active and inactive parts of the plate. This insight allows a plate design that can be effective longer and consequently leads to remarkable reduction in a number of NAM plates required in the process. Another key contribution of iDNAM is replacing a costly proprietary software with Blender, an open-source general 3D software suite. This has a great practical value for providing a more affordable alternative. Objectivewise, iDNAM has been shown to be clinically effective in the nasoalveolar molding treatment for patients with complete UCLP. [18–21]

Nonetheless iDNAM in its current state requires a personnel with both craniofacial expertise and proficiency in 3D computer modeling. To address this issue, our pilot investigation studies an automatic process to generate a bridge model---a crucial part in iDNAM-plate design---using mathematical modeling, data projection, and common CAD techniques. Section 2 provides a background on iDNAM. Section 3 elaborates on our proposed bridge model and its underlying generation process. Section 4 presents the assessment. Section 5 discusses and concludes the study.

2 individualize Digital NasoAveolar Molding

Digital technology has emerged as promising areas of craniofacial cleft care, particularly in NAM therapy. Individualized Digital NAM or iDNAM is a new digital NAM technique using a full digital workflow for NAM plate design and fabrication. Once the alveolar cleft gap reaches 3-4 mm, the patient can be scheduled for the primary lip surgery.

In the same spirit but with current technologies, recent studies [8, 9] replace impression taking and the conventional plate fabrication with an intraoral scanner and CAD/CAM technology for plate design and fabrication. However, to cope with progresses, either conventional or current digital NAM may require multiple adjustments or the use of multiple plates.

The iDNAM virtual setup is based on the differential force application [3–5], in which taping force results in plate rotation bringing the greater segment closer to the lesser segment. In the conventional NAM biomechanics, factors limiting plate rotation including the position of the retention button, the distal end of the plate, and the acrylic (the plate material) filling the cleft gap between greater and lesser segments can cause either multiple adjustments or the use of multiple plates throughout the course of treatment.

That is, the more functional rotation a plate can achieve, the fewer plates (or adjustments) are required. Thus, they propose individualized Digital NAM (iDNAM) with key distinctions, i.e., relocation of the retention button, using a shorter plate on the lesser segment side, and virtually removing of the palatal acrylic in the cleft gap. These factors bring the benefits of minimizing the number of plates used, but pose a challenge in digital plate design. One of the most notable challenges is automatically modeling a proper space volume between the greater and the lesser segments, such that this space volume can well accommodate progress throughout the course of the treatment. Section 3 discusses our hypotheses and approach to address this particular challenge.

3 Bridge Model

A plate design in iDNAM workflow requires a bridge model, a three-dimension surface connecting the greater and the lesser segments. Once a bridge model is finalized, it is then connected to other parts. The combination continues on in a plate design process, until a 3D-print-ready plate design is obtained.

The problem. To provide a bridge model is to recognize a pattern in a three-dimension (3D) surface data and generate a geometry shape.

Our proposed solution. With characteristics of an alveolar ridge---its path seems lying flat on an xy-plane and looks elliptic---, we propose a solution based on low-computation techniques: identify the ridge, approximate its path with ellipse, determine a proper cross-section and apply it uniformly along the path to create a 3D shape of the bridge model.

This seemingly straightforward approach has to overcome some technical challenges. (1) A predictive model can generally perceived as providing $y' = f(x; \omega)$ where

x and $\boldsymbol{\omega}$ represents model input and a parameter set. While in our case the data points are in xy-coordinates, this may look deceptively natural to have the model predict a *y* coordinate out of an *x* coordinate. This may be fine for many situations, but for an elliptic model this would lead to a half ellipse (not bad for the bridge model, which is likely to take only a small segment of an ellipse). However, with this cartesian view, it does not encourage cross-section visualization and could lead to a more complicated implementation down the road. (2) The bridge model has to be drawn upon the data of cross-sections. The cross-sections are taken at various locations along the path. Each consists of face coordinates. These coordinates are not uniformly spacing and the sizes of cross-sections vary largely along the path. It results in a dense cloud, almost solid-look, of combined cross-section data points, Fig. 4. The task seems simple as a human can effortlessly see the outline, but without the right perspective an efficient computational procedure to model the outline is not that simple.

Modeling the outline of this dense cloud is not a simple machine learning task either. E.g., an artificial neural network (ANN) for regression optimizing mean-square error is theoretically [22] to have the predictive model $f(x; \boldsymbol{\omega}) \approx E[y|x]$. Binary-classification ANN optimizing cross-entropy loss is to have $f(x; \boldsymbol{\omega}) \approx p(y=1|x)$, conditional probability[22]. Multi-class-classification ANN optimizes categorical cross-entropy loss. It is to have $f(x; \boldsymbol{\omega}) \approx [p(C_1 = 1|x, s), \ldots, p(C_K = 1|x, s)]^T$, a vector of conditional class probabilities[23, 24], where *x* is an input and *s* is the in-context condition, i.e., *x* belongs to one of the prepared classes (C_1 to C_K). Approximating an outline of a dense cloud---perhaps framed as $\min_{\omega} \Sigma_n f(x_n; \boldsymbol{\omega})$ s.t. $f(x_n; \boldsymbol{\omega}) \geq y_n$ for all *n*'s---is a different task. This challenge cannot be handled using the three major machine learning tasks. The rest of this section elaborates on how we overcome these challenges.

3.1 Input and Data

Given an Intra-Oral Scan (IOS) data (as an STL file, Fig. 1), the reference points and plane are assigned manually (Fig. 2). With reference points and plane assigned, axes and coordinates are consistent, e.g., alveolar ridge lays on an x-y plane, with origin (0, 0, 0) at the middle point between references T and T'.

The reference points. Postgingivale of greater segment, T, is defined as a junction of the crest of the ridge with the outline of the tuberosity of the greater segment. Canine point of greater segment, C, is defined as a crossing point of canine groove and alveolar ridge of the greater segment. Postgingivale of lesser segment, T', is defined as a junction of the crest of the ridge with the outline of the tuberosity of the lesser segment.

The input. The imported IOS shape is three-dimension (3D) geometry data described by vertices, edges, and faces. Only face information, particularly centers and normal vectors, are used for modeling and associate computation in our study. That is, data $\boldsymbol{D} = [\boldsymbol{c}_x, \boldsymbol{c}_y, \boldsymbol{c}_z, \boldsymbol{n}_x, \boldsymbol{n}_y, \boldsymbol{n}_z]$ where $\boldsymbol{c}_x$, $\boldsymbol{c}_y$, $\boldsymbol{c}_z$, represent coordinates of face center locations and $\boldsymbol{n}_x$, $\boldsymbol{n}_y$, $\boldsymbol{n}_z$ represent components of normal vectors. Note that a face also contains information of vertices and edges associated to it. This information tells the actual boundary of a face and whether a face shares vertex or edge boundaries with its neighbors, but this is not relevant to our task and discarded for simplicity.

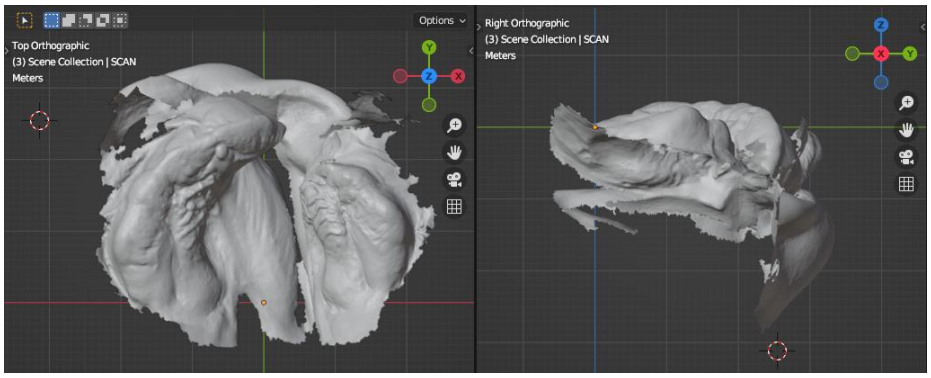

Fig. 1. A geometric shape obtained from the Intra-Oral Scan is imported and shown in multiple views, on Blender.

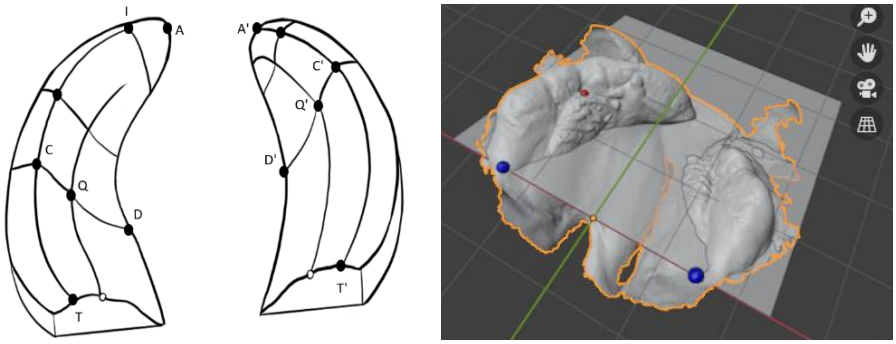

Fig. 2. Reference points and plane. (Left) Anthropometric landmarks. (Right) Reference points (T, C, and T' in order from left to right) and an x-y plane ($z = 0$) used in our study.

3.2 Ridge Identification and Approximation

The ridge is assumed to locate above the reference x-y plane (z > 0) with its top relatively flat and its inner and outer sides facing toward and away from the origin (0,0,0). That is, face $\boldsymbol{u}$ is taken as ridge, if its $c_z > 0$, where c_z is a z-coordinate of the face location.

In addition, we can further identify top, outer, and inner parts of the ridge, using vector operations. Given radial pointing to the face $\boldsymbol{\rho} = \boldsymbol{c} - \boldsymbol{c}_o$, where $\boldsymbol{c}$ and $\boldsymbol{c}_o$ are the face and origin locations, that ridge face $\boldsymbol{u}_r$ are taken as a top $\boldsymbol{u}_t$ if $| \boldsymbol{n} \times \boldsymbol{\rho} | > \tau$ (user-specific threshold) otherwise considered as an outer side $\boldsymbol{u}_o$ if $\boldsymbol{n} \cdot \boldsymbol{\rho} > 0$ or an inner side $\boldsymbol{u}_i$ if $\boldsymbol{n} \cdot \boldsymbol{\rho} < 0$. This classification is only used to understand the alveolar ridge. It is not used in our current proposed bridge model.

Once ridge faces $\boldsymbol{U}_r$ are identified, ridge data points are used to fit an ellipse model,

$$r' = \frac{c}{\sqrt{\frac{\cos^2(\theta)}{a^2} + \frac{\sin^2(\theta)}{b^2}}} \tag{1}$$

where (r', θ) are polar coordinates on the ellipse; a, b, and c are elliptic parameters. The cartesian location (x, y) of a ridge face is converted to the equivalent polar (r, θ). Specifically, the fitting is, $\min_{a,b,c} E$ where $E = \Sigma_n (r'(\theta_n; a,b,c) - r_n)^2$. Note z is discarded, $z_n = 0$ for all n's.

3.3 Cross-Section and The Bridge Model

A cross-section of the bridge model has to be able to accommodate the widest expand of the alveolar segment moving through it. Therefore, it is better to learn this cross-section from cross-sections of the alveolar ridge.

Fig. 3 (Right) and Fig. 4 (Right) show cross-sections of the alveolar ridge along the best-fit circle and ellipse, respectively. The cross-section visualization is produced by plotting $(r_n - r'(\theta_n), z_n)$ for every ridge datapoint, where $r'(\theta_n)$ is the corresponding point on the approximation, being either circle or ellipse.

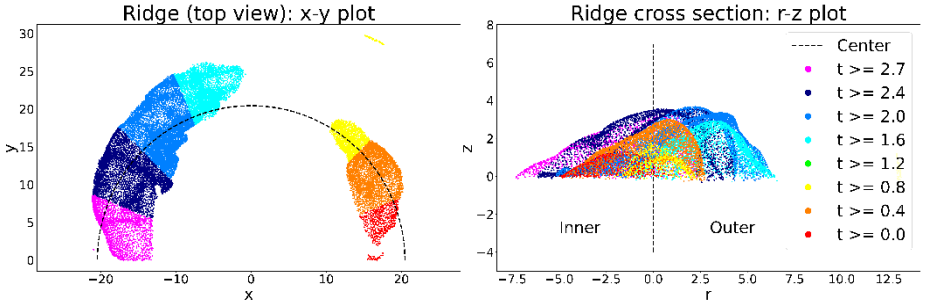

Fig. 3. Alveolar ridge cross-section seen along the best-fit circle. Left: the alveolar ridge from top view displayed in different colors. Each color marks data points located within a particular angular range, e.g., red for $0 \leq t < 0.4$ (in radian). Right: color-marked data points displayed in *r-z* reveal an outline of the cross-section of the alveolar ridge along the approximate ridge path, best-fit circle in this case. The dash line shows the approximate ridge path on the left plot and a center of the path on the right plot. The colors are just to illustrate the idea and disclose changes in cross-sections throughout the approximate ridge path.

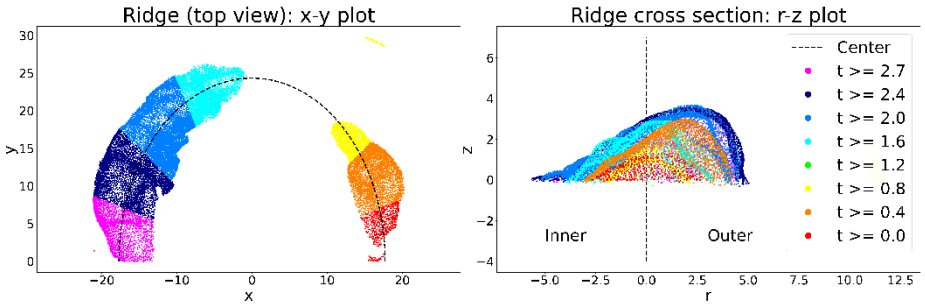

Fig. 4. Alveolar ridge cross-section seen along the best-fit ellipse. The left plot shows that the cross-sections at different locations are well aligned.

Since cross-sections of different parts seem to be more aligned when using ellipse, this indicates the virtue of an elliptic path approximating the alveolar ridge. The cross-section plots also reveal that the slope of the inner side of the ridge (r is smaller, closer to the origin) is much gentler than the slope of the outer side.

With the cross-section data $\{(r^*_n = r_n - r'(\theta_n),\ \theta_n,\ z_n)\}_{n=1,\ldots,N}$, the outline of the widest expand of the cross-section along the path can be approximated using discretization and linear piecewise model.

Discretization. Given the ridge data $\{(r^*_n,\ \theta_n,\ z_n)\}_{n=1,\ldots,N}$, a non-parametric cross-section model can be obtained through discretization, as follows. (1) For the selected number, M, the data is divided by values of r^* into $M-1$ equally-spacing bins. (2) Each bin is set to be as high as its maximum z. (3) A series of values of r^*'s and z_{max}'s makes up a discrete model. Specifically, given M, define $q_0 = \min(\boldsymbol{r^*})$ and $q_{M-1} = \max(\boldsymbol{r^*})$. Let $\boldsymbol{q} = [q_0, q_1, \ldots, q_{M-1}]$, where $q_m = q_0 + m\ (q_{M-1} - q_0)/(M-1)$ for $m = 1, \ldots, M-2$. Let $\boldsymbol{h} = [k_0, k_1, \ldots, k_{M-1}]$ where $k_m = \max\ \{\ z_n \mid n\colon q_m \le r^*_n < q_{m+1}\ \}$ for $m = 1, \ldots, M-2$ and $k_{M-1} = k_{M-2}$.

Linear piecewise model. The discrete model assures that its approximation is never smaller than the outline. This is the desired property, but the consequent roughness is undesirable. Thus, a linear piecewise model is constructed based on the discrete model. Note that a higher-degree spline function could be preferable, but a linear piecewise function is our choice for this pilot study.

Making a linear piecewise model out of $\boldsymbol{q}$ and $\boldsymbol{h}$ should be straightforward, as piecing together each point in the series. However, since the bridge model is supposed to be larger than (or at least equal to) the outline, this requires a correction at the peak (global maximum). That is, after the peak bin, the bin heights are shifted such that the peak height is repeated once. Specifically, the bin heights are corrected as, $\boldsymbol{h'} = [h_i]_{i=1,\ldots,M-1}$ where $h_i = k_i$ if $i \le \text{argmax}_i\ k_i$ otherwise $h_i = k_i - 1$.

In practice, these $\boldsymbol{q}$ and $\boldsymbol{h'}$ are enough to create a cross-section curve, which is a series of vertices in Blender, i.e., vertex coordinates can be defined as ($x_i = q_i$, $y_i = h_i$, $z_i = 0$). However, for academic completeness, this cross-section curve is equivalent to a linear piecewise model, $f_S(x;\ \boldsymbol{q},\ \boldsymbol{h'}) = h_i + (h_{i+1} - h_i)\ (x - q_i)/(q_j - q_i)$ where $q_i \le x < q_j$.

Data preparation process. Before going through the discretization process, the data $D^* = \{(r^*_n,\ \theta_n,\ z_n)\}_{n=1,\ldots,N}$ should be selected and cleaned such that it contains only what matters, i.e., within the functional angle $\theta \in [\ \alpha, \beta\ ]$ and without the outliers. The outliers can be defined as any datapoint whose $r^* <$ Q1 − 1.5 IQR or $r^* >$ Q3 + 1.5 IQR, where Q1 and Q3 are the 1st and 3rd quartiles, respectively. IQR is the interquartile range, IQR = Q3 − Q1.

Fig. 5 shows the approximation of the outline. Notice that a larger M associates to a more accurate outline.

The bridge model. To finalize the bridge model, the bridge path is obtained from ellipse model $r'(\theta)$ for $\theta \in [\theta_b, \theta_e]$. The starting and ending points can be specified, e.g., C and T' are used in our assessment. Then, the cross-section model $f_S(x;\ \boldsymbol{q},\ \boldsymbol{h'})$ is applied upon the bridge path using Blender bevel operation[25]. Fig. 6 shows the final outcome.

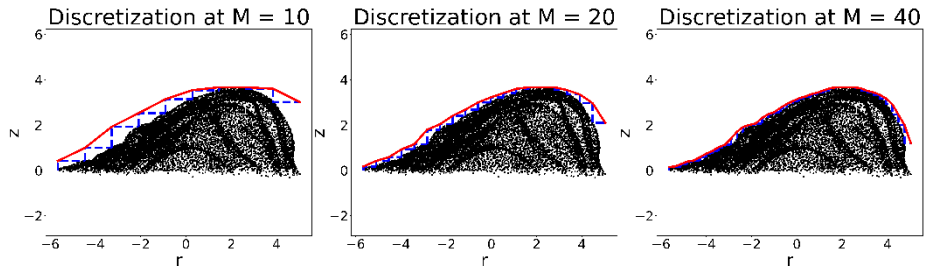

Fig. 5. Cross-section model by discretization. The higher discretized resolution (the larger *M*) is, the closer the approximation is to the outline of the cross-section data.

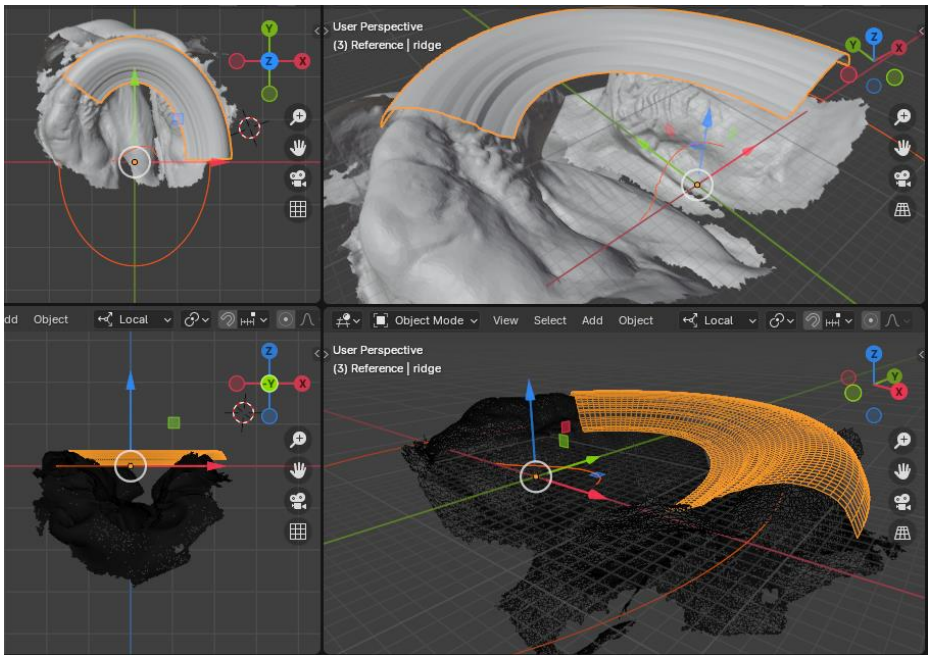

Fig. 6. The bridge model, displayed along with the intra-oral scanned shape, the cross-section and elliptic models. (The bridge, cross-section, and elliptic models are highlighted in orange). Upper row displays in solid mode. Lower row displays in wireframe mode.

4 Assessment

A sample of the intra-oral scanned shape from a cleft-lip patient was the subject of our pilot study. Our method processed the information as elaborated in Section 3 and then provided the bridge model (using discretization $M = 30$). The bridge model was assessed by the craniofacial experts. Two experts had participated. Table 1 shows their assessments.

Table 1. Experts' opinions on the resulting bridge model

Assessment	Opinion	Remark
Overall	6.5	Expert 1
(score out of 10)	7	Expert 2
	6.75	Average
What's good?	(1) The model's ability to approximate and simulate an ideal arch form of infants without clefts. (2) Utilizes the outermost anatomy of the ridges to allow free rotation of the plate and natural growth.	Expert 1
	(1) The height of the bridging model is aligned with the maximum areas of alveolar ridges. (2) The starting and ending points of this models can be adjusted.	Expert 2
What's lacking?	(1) Vertical extension of the plate at the buccal and palatal side adjacent to the cleft site. (2) The ability to modify the extension of the bar on the lesser segment (consider changing t' to c' or use other reference points on the lesser segment to see the most appropriate terminal point)	Expert 1
	(1) The extension of the bridging model is not covering the depth of the alveolar segments. (2) The edge is still sharp, and it will require the smoothen steps. (3) The width of the model is larger on the cleft side.	Expert 2
Comments	Consider changing the name from proto-plate to bridge model.	Expert 1
	Due to the starting point is based on T-T' and horizontal plane and the vertical extension extending only in Z-positive axis, thus it should include the Z-negative value to extend the bridging model to cover the anatomical landmark of the alveolar ridges.	Expert 2

To complement the experts' opinions, Blender operations and durations to perform comparable tasks were counted and timed. An expert had participated. The results are shown in Table 2.

Table 2. Blender operations and performing times on tasks

Method	Measure	Reference preparation	Bridge modeling
Mirror method	Time	1 min	6 min
	#operations	64	74
Our method	Time	3 min	2 sec
	#operations	53*	N/A

* It involves an auxiliary script that may make a number of operations appear much different than the actual one.

Note (1) operation counts and performing durations may vary widely due to various reasons. Many of them may not reflect any quality of the methods under investigation. Use of statistics may alleviate the issue, but due to the very personnel issue we intend to mitigate, it is difficult to find qualified experts to participate. (2) The entries with N/A reflect that the task has been performed completely by running our program. A number of operations is not apparent to count in this case. (3) The expert participated in this assessment has about 2-year experience in 3D computer modeling. The short performing times well reflect her proficiency. (4) The working times are presented here is just to somewhat provide an objective information on how difficult the task is. Our main goal is to address the personnel issue in iDNAM. The speed up if it really happens is only a by-product. (5) Some interaction in Blender may result in many operations behind the scene. Hence, a number of operations may not always reflect how difficult the task really is, from a practitioner's perspective.

5 Discussion and Conclusion

The assessment shows that our approach is in the right direction. Both elliptic path and cross-section models have received positive reviews. There are some aspects need to be worked out. (1) The insufficient coverage of the bridge model, particularly in the z-direction (currently no coverage at all for $z \leq 0$). (2) A functional angular range, currently between C and T', is too wide and this should be adjustable, in practical usage. (3) The bridge model needs to be smooth.

Regarding the key mechanisms, the elliptic path and cross-section models have provided a satisfactory outcome and can finish the task quickly. This shows viability of this low-computation approach in generating a 3D-surface bridge model. In addition, the finding also supports our hypothesis of an elliptic pattern of an alveolar ridge.

However, these mechanisms rely on provided reference points and plane. Providing these references manually or semi-automatically still requires some degree of 3D modeling skills. Propitiously, recent works [26, 27] have shown an impressive result on landmark localization. Along with refining our bridge model, integration with landmark localization and automation of the later processes (till a print-ready design) are the road head toward our long-term goal.

This article proposed a bridge model using elliptic and non-parametric cross-section models. The approach has been assessed to be fairly good with positive comments on the key mechanisms, but still need quite a few improvements on many details.

6 Acknowledgement

We are greatly appreciated Wasu Chaopanon for his support for the project, valuable comments and major development of Blender scripts and add-ons.

References

1. Mossey PA, Little J, Munger RG, et al (2009) Cleft lip and palate. The Lancet 374:1773–1785. https://doi.org/10.1016/S0140
2. Figueroa AA, Polley JW (2005) Orthodontics in Cleft Lip and Palate Management. pp 271–310
3. Grayson BH, Maull D (2004) Nasoalveolar molding for infants born with clefts of the lip, alveolus, and palate. Clin Plast Surg 31:149–158
4. Shetye PR, Grayson BH (2017) NasoAlveolar molding treatment protocol in patients with cleft lip and palate. Semin Orthod 23:261–267. https://doi.org/10.1053/j.sodo.2017.05.002
5. Grayson BH, Shetye PR (2009) Presurgical nasoalveolar moulding treatment in cleft lip and palate patients. Indian Journal of Plastic Surgery 42
6. Grayson BH, Santiago PE (1999) Presurgical Nasoalveolar Molding in Infants with Cleft lip and Palate. Cleft Palate-Craniofacial Journal 36:486–498. https://doi.org/10.1597/1545-1569(1999)036<0486:PNMIIW>2.3.CO;2Source
7. K. Matsuo and T. Hirose (1991) Preoperative Non-Surgical Over-Correction of Cleft Lip Nasal Deformity. Journal of Plastic Surgery 44:5–11
8. Zarean P, Zarean P, Thieringer FM, et al (2022) A Point-of-Care Digital Workflow for 3D Printed Passive Presurgical Orthopedic Plates in Cleft Care. Children 9:. https://doi.org/10.3390/children9081261
9. Carter CB, Gallardo FF, Colburn HE, Schlieder DW (2022) Novel Digital Workflow for Nasoalveolar Molding and Postoperative Nasal Stent for Infants With Cleft Lip and Palate. Cleft Palate-Craniofacial Journal. https://doi.org/10.1177/10556656221095393
10. Zheng J, He H, Kuang W, Yuan W (2020) Novel Three-Dimensional Coordinate System to Analyze Alveolar Molding Effects of Pre-Surgical Nasoalveolar Molding on Infants With Non-Syndromic Unilateral Cleft Lip and Palate. J Craniofac Surg 31:653–657. https://doi.org/10.1097/SCS.0000000000006148
11. Al Khateeb KA, Fotouh MA, Abdelsayed F, Fahim F (2021) Short-Term Efficacy of Pre-surgical Vacuum Formed Nasoalveolar Molding Aligners on Nose, Lip, and Maxil-lary Arch Morphology in Infants With Unilateral Cleft Lip and Palate: A Prospective Clinical Trial. Cleft Palate-Craniofacial Journal 58:815–823. https://doi.org/10.1177/1055665620966189
12. Schiebl J, Bauer FX, Grill F, Loeffelbein DJ (2020) RapidNAM: Algorithm for the Semi-Automated Generation of Nasoalveolar Molding Device Designs for the Presur-gical Treatment of Bilateral Cleft Lip and Palate. IEEE Trans Biomed Eng 67:1263–1271. https://doi.org/10.1109/TBME.2019.2934907
13. Abd El-Ghafour M, Aboulhassan MA, Fayed MMS, et al (2020) Effectiveness of a Novel 3D-Printed Nasoalveolar Molding Appliance (D-NAM) on Improving the Max-illary Arch Dimensions in Unilateral Cleft Lip and Palate Infants: A Randomized Controlled Trial. Cleft Palate-Craniofacial Journal 57:1370–1381. https://doi.org/10.1177/1055665620954321
14. Zheng J, He H, Kuang W, Yuan W (2019) Presurgical nasoalveolar molding with 3D printing for a patient with unilateral cleft lip, alveolus, and palate. American Journal of Orthodontics and Dentofacial Orthopedics 156:412–419. https://doi.org/10.1016/j.ajodo.2018.04.031
15. Bous RM, Kochenour N, Valiathan M (2020) A novel method for fabricating nasoalveolar molding appliances for infants with cleft lip and palate using 3-dimensional workflow and clear aligners. American Journal of Orthodontics and Den-tofacial Orthopedics 158:452–458. https://doi.org/10.1016/j.ajodo.2020.02.007

16. Batra P, Gribel BF, Abhinav BA, et al (2020) OrthoAligner “NAM”: A Case Series of Presurgical Infant Orthopedics (PSIO) Using Clear Aligners. Cleft Palate-Craniofacial Journal 57:646–655. https://doi.org/10.1177/1055665619889807
17. Yu Q, Gong X, Shen G (2013) CAD presurgical nasoalveolar molding effects on the maxillary morphology in infants with UCLP. Oral Surg Oral Med Oral Pathol Oral Radiol 116:418–426. https://doi.org/10.1016/j.oooo.2013.06.032
18. Parakarn H, Pisek P, Wangsrimongkol B (2023) iDNAM: ADVANCEMENTS IN CRANIOFACIAL CLEFT CARE THROUGH CAD/CAM. In: Joint 37th IADR-SEA Annual Scientific Meeting and 2nd International Oral Health Symposium. Interna-tional Association for Dental Research - Southeast Asia Division (IADR-SEA), Singapore, pp 263–263
19. Parakarn H, Pisek P, Wangsrimongkol B (2023) A new perspective of digital nasoalveolar molding therapy in patients with complete cleft lip and palate. Europe-an Journal of Orthodontics EOS2023 abstracts 45:e1–e419
20. Parakarn H, Pisek P, Wangsrimongkol B (2023) A Novel Digital NAM on Improving Alveolar Ridges and Nasal Morphology in Patients with UCLP. In: The 56th Annual Scientific Congress of the Korean Association of Orthodontists. Korean Federation of Science and Technology Societies (KOFST), Korea, pp O05–O05
21. Parakarn H, Winaikosol K, Pisek P, Wangsrimongkol B (2022) A revolutionary concept of 3D-printed individualized Digital NasoAlveolar Molding (iDNAM) for patients with complete unilateral cleft lip and palate. In: 14th International Congress of Cleft Lip and Palate and Related Craniofacial Anomalies. 14th International Cleft Congress, Edinburgh, UK
22. Bishop, C.: Pattern Recognition and Machine Learning. Springer (2006)
23. Nakjai, P., Ponsawat, J., Katanyukul, T.: Latent cognizance: What machine really learns. In: 2nd International Conference on Artificial Intelligence and Pattern Recognition, Beijing, China, pp 164–169. ACM (2019).
24. Katanyukul, T., Nakjai, P.: Recognition awareness: adding awareness to pattern recognition using latent cognizance. Heliyon 8(24), e09240 (2022).
25. Blender Manual, https://docs.blender.org/manual/en/latest/modeling/meshes/editing/edge/bevel.html, last accessed 2023/12/14.
26. Payer, C., Štern, D., Bischof, H., Urschler, M.,: Regressing Heatmaps of Multiple Landmark Localization Using CNNs. 19th International Conference on Medical Image Computing and Computer-Assisted Intervention, Athens, Greece, pp 230–238 (2016).
27. Wu, T.-H., Lian, C., Lee, S., Pastewait, M. F., Piers, C., Liu, J., Wang, F., Wang, L., Chiu, C.-Y., Wang, W., Jackson, C. B., Chao, W.-L., Shen, D., Ko, C.-C.: Two-Stage Mesh Deep Learning for Automated Tooth Segmentation and Landmark Localization on 3D Intraoral Scans. IEEE Transactions on Medical Imaging 41, pp 3158-3166 (2021)